ADVANCED MATERIALS
www.advmat.de

Toward Thin-Film Laser Diodes with Metal Halide Perovskites

Iakov Goldberg, Karim Elkhouly, Nirav Annavarapu, Sarah Hamdad, Maider Calderon Gonzalez, Jan Genoe, Robert Gehlhaar, and Paul Heremans**

Metal halide perovskite semiconductors hold a strong promise for enabling thin-film laser diodes. Perovskites distinguish themselves from other non-epitaxial media primarily through their ability to maintain performance at high current densities, which is a critical requirement for achieving injection lasing. Coming in a wide range of varieties, numerous perovskites delivered low-threshold optical amplified spontaneous emission and optically pumped lasing when combined with a suitable optical cavity. A progression toward electrically pumped lasing requires the development of efficient light-emitting structures with reduced optical losses and high radiative efficiency at lasing-level current densities. This involves a set of important trade-offs in terms of material choice, stack and waveguide design, as well as resonator integration. In this Perspective, the key milestones are highlighted that have been achieved in the study of passive optical waveguides and light-emitting diodes, and these learnings are translated toward more complex laser diode architectures. Finally, a novel resonator integration route is proposed that is capable of relaxing optical and electrical design constraints.

1. Introduction

The photonics industry greatly relies on photonic integrated circuits (PIC) to generate, detect, modulate, and process light over a broad spectrum from ultraviolet to infrared wavelengths. In the state of the art, integration of laser diode sources onto PICs is done by heterogenous integration techniques.[1] The next step in PIC development is the monolithic integration of electrically pumped coherent light sources. Non-epitaxial thin films are a promising candidate to fill this gap owing to their numerous benefits over conventional III-V semiconductors.[2] These advantages include low-temperature processing, broad substrate compatibility, chemical versatility, and ease of processing.[3,4] Currently, thin-film lasers, based typically on organic, colloidal quantum dots (QD), or metal halide perovskite semiconductors, operate in practice by optical excitation and therefore rely on an external light source for pumping to the lasing threshold. The desired transition to electrical pumping has been the subject of numerous studies and is not adequately solved yet.[5–10] Indeed, delicate trade-offs and complex optoelectronic design requirements must be met, to cope with the low electrical and thermal conductivities of these thin-film material systems and to deal with specific loss mechanisms such as Auger recombination and free carrier absorption losses. Nonetheless, after multi-decade research efforts, several critical breakthroughs have been achieved. These include the demonstration of electrically pumped amplified spontaneous emission (ASE) from continuously graded colloidal QDs,[11] and the realization of an organic laser diode under direct,[12] and indirect[13] electrical pumping schemes. However, the reliability and performance of these devices leave much to be desired, triggering interest in other non-epitaxial systems.

Metal halide perovskites, hereafter referred to as perovskites, while excelling in applications such as solar cells,[14–16] LEDs,[17–20] and photodetectors,[21,22] have yet to unveil their full potential as a laser gain medium. Perovskites exhibit several unique properties that distinguish them from other thin-film contenders. These include ambipolar charge carrier mobilities exceeding 10 $cm^2\ V^{-1}\ s^{-1}$,[23] Auger recombination rates in the range between 10^{-26}–$10^{-29}\ s^{-1}\ cm^6$,[24,25] along with competitive material gain values up to $10^4\ cm^{-1}$.[26] Simultaneously, perovskites display major drawbacks that limit their electrical performance at high bias onsets, such as low damage thresholds, operational instability,[27,28] ion migration,[29] or degradation via redox chemistry.[30,31] Our aim in this Perspective is to highlight the key photophysical and optoelectronic properties of perovskites that render them promising candidates for lasing applications and to

I. Goldberg, K. Elkhouly, N. Annavarapu, S. Hamdad, M. C. Gonzalez, J. Genoe, R. Gehlhaar, P. Heremans
IMEC
Kapeldreef 75, Leuven 3001, Belgium
E-mail: robert.gehlhaar@imec.be; paul.heremans@imec.be
I. Goldberg, K. Elkhouly, N. Annavarapu, S. Hamdad, M. C. Gonzalez, J. Genoe, P. Heremans
ESAT, KU Leuven
Kasteelpark Arenberg, Leuven 3001, Belgium

The ORCID identification number(s) for the author(s) of this article can be found under https://doi.org/10.1002/adma.202314193

DOI: 10.1002/adma.202314193

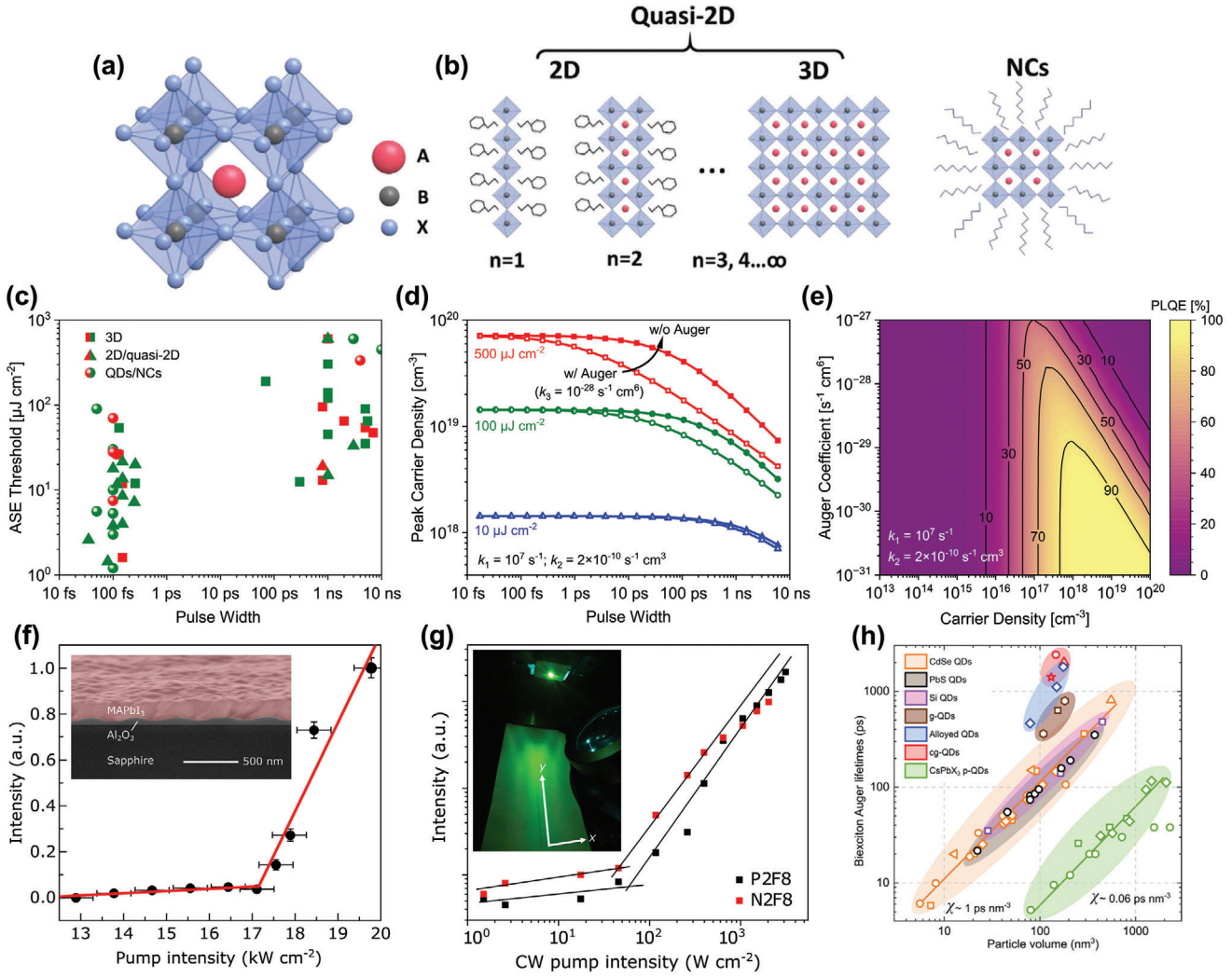

Figure 1. Metal halide perovskites for optically excited ASE and lasing. a) Perovskite crystal structure and b) various morphologies. Reproduced with permission.[32] Copyright 2021, John Wiley and Sons. c) ASE thresholds as a function of optical pulse widths. For details of each data point see Table S1 (Supporting Information). d) Peak N extracted by solving the rate equation (Equation (2)) with ($k_3 = 10^{-28}$ s^{-1} cm^6) and without Auger contribution. The horizontal axis refers to the full width at half maximum of a Gaussian optical pulse. e) PLQY as a function of N and k_3 recombination coefficient. In (d) and (e), k_1 and k_2 were fixed at 10^7 s^{-1} and 2×10^{-10} s^{-1} cm^3, respectively. f) CW DFB lasing from a mixed-phase system at ≈102 K. Inset: Laser structure. Reproduced with permission.[41] Copyright 2017, Springer Nature. g) CW DFB lasing intensity for quasi-2D perovskites with different organic cations at RT. Inset: Far-field lasing pattern. Reproduced with permission.[42] Copyright 2020, Springer Nature. h) Volume scaling of biexciton Auger lifetimes for NCs and QDs of variable compositions. Perovskites are highlighted in green. χ is a proportionality constant that connects QD volume and biexciton Auger lifetime. Reproduced with permission.[43] Copyright 2023, American Chemical Society.

propose guidelines for designing device architectures that could enable perovskite laser diodes.

Broadly, perovskites can be categorized into three groups with distinct properties: a) 3D; b) 2D or quasi-2D; and c) 0D. These configurations can be either hybrid organic-inorganic or purely inorganic compositions (**Figure** 1a,b).[32] A formula ABX_3 can be ascribed to the 3D perovskites, where A is a 12-fold-coordinated monovalent cation such as methylammonium (MA^+), formamidinium (FA^+), or cesium (Cs^+), among others; B is a six-fold-coordinated inorganic divalent inorganic cation (mostly Pb^{2+} or Sn^{2+}); and X is a strongly electronegative monovalent halide anion (I^-, Br^-, or Cl^-). Archetypical 3D perovskites exhibit poor photoluminescence quantum yield (PLQY) under weak excitation intensities (<10^{15} cm^{-3}),[33] owing to low bimolecular radiative recombination (k_2) rates relative to monomolecular non-radiative (k_1) rates. A more excitonic-like recombination character can be promoted by introducing bulky aromatic or aliphatic cations into the A-site to segregate the inorganic octahedra and obtain layered perovskites with 2D ($n = 1$ polymorph with the highest bandgap) or quasi-2D ($n > 1$) morphology, where n denotes the number of inorganic $[BX_6]^{4-}$ octahedral layers between the organic barriers.[34] Highly oriented 2D domains allow for fast (<0.5 ps) energy funneling along cascaded energy levels, which was shown to be important for efficient perovskite LEDs (PeLEDs).[35] Finally, 0D perovskite nanocrystals (NCs) and QDs can have their optoelectronic properties engineered

through quantum confinement, producing narrow (<100 meV) and highly size-dependent emission.[36–38] Being comparable to or larger than their Bohr radius, NCs can be weakly confined and bear the attributes of bulk semiconductors.[39,40]

2. Benchmarking Optical Gain

Among many properties of various perovskite polymorphs, a higher optical gain is crucial for lasing. The high photostability of many perovskite semiconductors when excited using either intermittent[44] or continuous wave (CW)[42,45] excitation makes optical measurements very potent. For example, intrinsic material gain (g_i) can be determined through ultrafast techniques such as transient absorption spectroscopy; however, the underlying gain mechanisms are often not straightforward to interpret.[39] Another question is how these mechanisms establish themselves under qualitatively different electrical driving, where the amplification along the inverted path would rely on the probabilistic spontaneous emission of photons by the material itself rather than on the photons supplied by the probe during the pump-probe experiments.[46]

Optical gain can arise from a degenerate electron-hole plasma or from the recombination of multiexcitons, such as biexcitons and trions. When constructing carrier-exciton phase diagrams, one must consider excitation intensity,[47] temperature,[48] and spatial carrier distribution.[49] Absent many-body effects, the ratio between multiexciton and free-carrier populations is adequately described by the Saha-Langmuir equation,[48] which points to the dominance of free carriers in systems with low exciton binding energy, at higher temperatures, and at low excitation intensities. Nonetheless, both free-carrier and excitonic gain bands can manifest in the same material under diverse conditions.[50]

An archetypical 0D semiconductor can be described as a two-level system with two-fold spin-degenerate states. The strong spatial confinement increases the overlap between the electron and hole wavefunctions, thereby enhancing the Coulomb interaction and promoting the formation of stable excitons. Excitation of a single exciton results in optical transparency, where stimulated emission is offset by absorption. To achieve population inversion, a second electron must be excited across the energy gap, forming a biexciton state. This implies that a semiconductor ensemble must have an average number of excited species greater than one. Driven by reduced optical density of states, threshold carrier density (N_{th}) can be lower in such confined systems. On the downside, maximum g_i is also lower due to rapid gain saturation, which would restrict lasing to low-optical-loss structures and would limit optical power output.[43]

A critical consequence of spatial confinement is the efficient non-radiative Auger recombination, which quickly depletes multiexcitonic gain on a sub-ns scale. As discussed further in the text, this would raise the lasing threshold, especially for practically useful (long) stimuli. In colloidal QDs, heterostructure and composition engineering were pivotal in extending Auger lifetimes and creating favorable conditions for single-exciton gain.[51-53] However, extending such strategies to perovskite systems is complicated by the high migration mobility of the halide anions,[54] suggesting that new routes are required for engineering perovskite QDs and NCs.

While the Saha-Langmuir equation suggests that the ratio of free carriers to excitons moves in favor of excitons toward higher excitation intensities, it does not account for exciton dissociation that occurs in the presence of free carriers as well as other Coulombic potentials. A sizeable transition from an excitonic system to electron-hole plasma occurs around the critical carrier density, known as Mott transition density, which is higher for excitons with smaller Bohr radius and stronger binding energy.[55] Thereby, the Mott transition is improbable in systems operating in a strong confinement regime. However, multiexciton to free-carrier transition, and hence free-carrier optical gain, were observed in more intermediate cases such as weakly confined $CsPbBr_3$ NCs,[39] opposite from other reports that highlight the excitonic nature of gain in comparable systems.[56,57]

In 3D perovskites, lower exciton binding energies and higher dielectric constants favor the generation of free charge carriers, which come with reduced non-radiative carrier recombination rates. Despite limited spectral tunability, these materials offer continuous spectral bands and high gain coefficients stemming from the high optical density of states. In contrast, the origin of optical gain in quasi-2D perovskites is subject to debate. The excitonic character of gain is dominant for low mean n ($\langle n \rangle$) compositions with high exciton binding energies,[58] while a combination of free carriers and excitons can be observed for quasi-2D perovskites with intermediate and high $\langle n \rangle$. Despite being significantly brighter at low excitation intensity, low-$\langle n \rangle$ quasi-2D compositions have demanded higher N_{th} relative to their 3D counterparts, triggered by a significant exciton-exciton annihilation (EEA).[59] Accumulation of non-emissive triplets in quasi-2D perovskites under long-pulse photoexcitation may further contribute to EEA.[42] Additionally, optical excitation fails to account for free charge carriers present under electrical driving, which would likely impede optical gain through exciton-charge annihilation. Regardless of the exact gain mechanisms in these quasi-2D systems, control over bandgap distribution and domain orientation could offer a strategy to produce materials with low N_{th} and high g_i.[60]

ASE-based experiments such as variable stripe length[61] or scattered emission profile[62] have been popular in the literature due to the ease of experimentation and are suited to extract the net gain (g_{net}) of the waveguide and N_{th}, yet they fail to elucidate the fundamentals of optical gain mechanisms. Although N_{th} can be determined at the onset of ASE, many publications mention only the ASE threshold and not the corresponding N_{th}.[32,63,64] Figure 1c presents ASE thresholds for perovskite films placed on passive substrates when excited using optical pulses from femtosecond (fs) to nanosecond (ns) range. The thresholds vary widely when using similar pulse widths (T_{pulse}), even in perovskites with comparable morphology and composition. Differences in absorption, excitation wavelength, waveguide, and pump geometry, and ASE extraction procedure contribute to the wide spread of reported values.[65–67] In particular, the discrepancies in excitation spot dimensions can cause major deviations.

The lowest ASE thresholds (< 10 μJ cm^{-2}) were predominantly reported under fs excitation, where carriers are excited instantaneously relative to their recombination lifetime ($\tau_{carrier}$). Under fs

conditions, it is possible to directly convert ASE threshold fluence (F_{th}) into N_{th}:[68]

$$N_{th} = \frac{F_{th} \cdot Abs}{\hbar\omega \cdot d} \quad (1)$$

where *Abs* is the fraction of absorbed incident light by the active layer, $\hbar\omega$ is the laser excitation energy, and d is the perovskite layer thickness. On the other hand, when T_{pulse} is comparable to or exceeds $\tau_{carrier}$, one can employ the simplified rate equation to analyze carrier generation-recombination dynamics and estimate carrier density (N) within a film at a given fluence:[68]

$$\frac{dN}{dt} = G - k_1 \cdot N - k_2 \cdot N^2 - k_3 \cdot N^3 \quad (2)$$

where G is the time-dependent carrier generation rate, k_1 is the monomolecular recombination coefficient (non-radiative), k_2 is the bimolecular recombination coefficient (radiative), and k_3 is the three-body Auger recombination coefficient (non-radiative). These free-carrier rates are specific to each device stack and can be determined using spectroscopic techniques while accounting for the relevant excitation intensities and ambient conditions. Importantly, **Equation (2)** is applicable under the assumption that the hole and electron densities are equal, and their recombination is non-excitonic. Here and below, similar quadratic differential equations can be drawn for excitonic perovskites, with second-order recombination assigned to EEA.[69]

By applying mid-range $k_1 = 1 \times 10^7$ s^{-1} and $k_2 = 2 \times 10^{-10}$ s^{-1} cm^3 values of an exemplary 3D perovskite and first disregarding Auger quenching processes, we extract the peak N within the film as a function of the optical pulse width for a range of excitation fluences (Figure 1d). A higher N can be achieved when using short T_{pulse} below 100 ps. In this ultrafast excitation regime, the active medium is quickly populated with carriers that build up during the pulse, giving rise to ASE that takes place on the ps scale.[70] Toward longer T_{pulse}, carrier recombination becomes more relevant, yielding lower N in the gain layer. These temporal differences between excitation pulses are exacerbated when accounting for Auger recombination, in particular at higher excitation fluences. Auger loss with a rate of $k_3 = 1 \times 10^{-28}$ s^{-1} cm^6 remains insignificant for ns-long pulses with a fluence of 10 μJ cm^{-2}, while reducing attainable N for 500 μJ cm^{-2} excitation delivered over hundreds of fs.

These results are consistent with the large difference between ASE thresholds under fs and ns excitations of 0D perovskites, whose short Auger recombination lifetimes have been well documented.[71,72] Being a non-radiative process, Auger recombination competes with radiative recombination, leading to a significant reduction in PLQY. Figure 1e shows a PLQY map of a perovskite film for different N and k_3 rates. By incorporating the k_1 and k_2 coefficients outlined above, we calculate PLQY according to:[73]

$$\mathrm{PLQY} = \frac{k_2 N^2}{k_1 N + k_2 N^2 + k_3 N^3} \quad (3)$$

In the low excitation regime (<10^{16} cm^{-3}), k_1 is the dominant carrier loss mechanism. Progressing toward 10^{17}–10^{18} cm^{-3}, PLQY starts to be governed by generally high k_2 for perovskites, which is comparable to that of III-V semiconductors.[74–76] k_3 rate surpasses radiative recombination beyond some critical carrier density N_C, where PLQY is 50%, such that $k_2 = k_3 N_C$. Under (quasi)-steady-state conditions, i.e., long excitations, the ASE threshold can be sustained only if N_{th} remains below N_C.[77]

The electrical modulation speed of state-of-the-art PeLEDs is currently limited to some ns,[78] making optical results derived using extremely short T_{pulse} less relevant toward current-injection lasing. CW optical ASE and lasing, where $T_{pulse} \gg \tau_{carrier}$, are considerably more representative when drawing parallels between optical and electrical stimuli, as CW optical excitation is associated with lower peak N and more pronounced local heating.[79] Consequently, the demonstration of CW ASE and lasing from 3D perovskites have been restricted to cryogenic temperatures (Figure 1f). Lower temperatures have enabled carrier funneling between different bandgap regions triggered by phase transition,[41] or have extended carrier lifetimes and exponentially reduced N_{th} in single-phase perovskites.[45]

At room temperature (RT), the most prominent CW results were reported for quasi-2D $FAPbBr_3$-based gain media with <n> of 8. CW distributed feedback (DFB) lasing was observed at a threshold as low as 45 W cm^{-2} (Figure 1g), highlighting long-lived triplet exciton accumulation as a primary obstacle under CW conditions.[42] Similarly to organic gain media, triplet annihilation could be addressed by introducing triplet quenchers.[80] Charge funneling gives rise to locally high N, while the remaining perovskite volume remains uninverted. This is in contrast to phase-stable 3D perovskites that display g_{net} across the entire volume, giving rise to more predictable modal gain distribution.

To the best of our knowledge, no true CW ASE or lasing has been demonstrated from perovskites with 0D morphology. Higher exciton binding energy of 0D semiconductors gives rise to enhanced Coulombic electron-hole interaction and consequently more efficient Auger recombination.[71,72] The Auger decay lifetimes are shown to be proportional to the NC volume, following a universal "volume scaling" law (Figure 1h). Perovskite QDs and NCs have been characterized by markedly shorter Auger recombination lifetimes than those derived from more traditional semiconductors, in particular from colloidal CdSe-based QDs.[43] Consequently, as of today, quasi-2D and 3D perovskites offer a more viable route to injection-lasing than 0D perovskite semiconductors.

3. Electrical Injection in PeLEDs

Optical gain measurements performed over simple waveguides can be used to screen diverse perovskite compositions. However, the path to electrical pumping requires equipping these perovskite layers with charge-selective transport layers and contacts with suitable energy bandgaps, band offsets, and interfacial properties. This is commonly achieved in a vertical PeLED architecture (**Figure 2a**). An accessible PeLED metric is the external quantum efficiency (EQE) as a function of current density (J). The EQE is the ratio of the number of photons that are emitted by the source into the forward-viewing hemisphere over the number of injected electrons.[81] Light outcoupling efficiency ($f_{outcoupling}$) connects EQE to internal quantum efficiency (IQE), which in turn

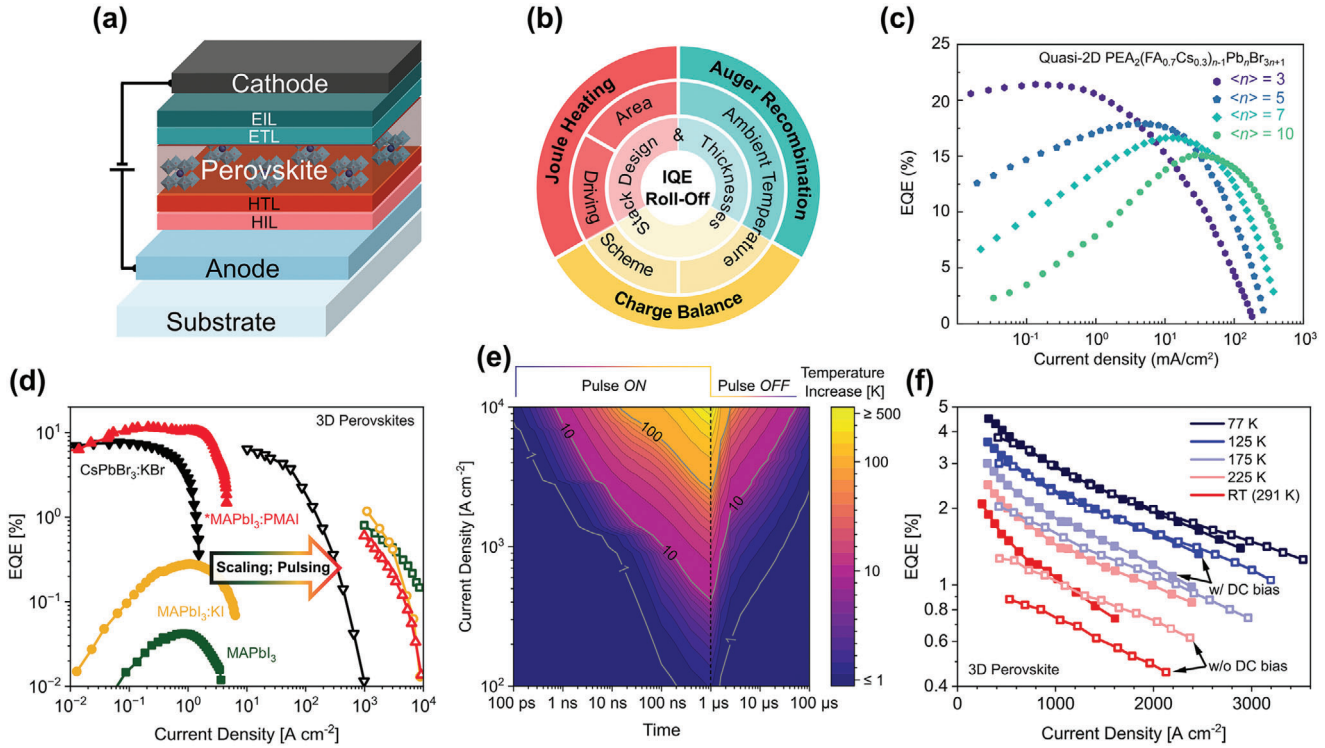

Figure 2. Performance of PeLEDs comprising quasi-2D and 3D perovskite emissive layers. a) Generic PeLED structure. HIL: hole injection layer. HTL: hole transport layer. ETL: electron transport layer. EIL: electron injection layer. Dimensions are not to scale. b) Relevant IQE roll-off mechanisms. c)DC EQE-*J* characteristics of quasi-2D PeLEDs. Reproduced with permission.[91] Copyright 2021, Springer Nature. d) DC (filled) and pulsed (unfilled) EQE-*J* characteristics of 3D PeLEDs. *$MAPbI_3$:PMAI thickness was changed from 40 to 80 nm when transitioning to pulsed measurements. Data points from refs. [78,93] e) Transient heat simulation. The pulse is sharply terminated after 1 µs. Model details are in Figure S1 (Supporting Information). f) Pulsed EQE-*J* characteristics at different temperatures acquired using DC bias (filled) and without DC bias (unfilled). Reproduced with permission.[100] Copyright 2022, John Wiley and Sons.

depends on PLQY, charge carrier balance efficiency ($f_{balance}$), and the probability of forming a correlated electron-hole pair $f_{e\text{-}h}$:[82]

$$EQE = IQE \times f_{outcoupling} = f_{balance} \times f_{e-h} \times PLQY \times f_{outcoupling} \quad (4)$$

Outcoupling-limited EQEs beyond 20%, corresponding to near-unity IQE, have been extracted from green,[83] red,[84] and near-infrared PeLEDs.[85] However, such IQEs were achieved in rather low current density regimes in the range of mA cm^{-2}, and by introducing elaborate passivation strategies that reduce k_1.[86–88] Toward higher current densities, relevant for injection-lasing, PeLEDs typically display a decrease in electroluminescence (EL) efficiency, known as roll-off, which can typically be caused by Auger recombination, Joule heating, and charge imbalance (Figure 2b).[89,90] The latter two mechanisms play a minor role in optical studies as both types of charge carriers are generated simultaneously upon a fast optical excitation, in addition to the limited heat generation in optical pumping experiments.

In PeLEDs, the contribution of each of the three mechanisms heavily depends on the stack design and the intrinsic properties of the perovskite emitter. Some of the lowest reported ASE thresholds (Figure 1c) have been obtained from quasi-2D perovskites. It is therefore useful to examine their electrical performance, in order to assess their suitability for electrically pumped lasing. From optical measurements, it was inferred that in quasi-2D perovskites, Auger quenching limits PLQY, and hence IQE, for a mean carrier density *N* larger than ≈10^{17} cm^{-3}.[91] It should be noted that in quasi-2D perovskites, there is effective carrier funneling toward lower-bandgap regions, as discussed earlier, such that the local *N* can be significantly larger than the mean *N*. This could indeed explain the occurrence of Auger recombination at relatively low mean *N*, corresponding to an apparently large k_3. A second observation is that EQE roll-off is reported to be more severe for compositions with a lower <*n*> or higher exciton binding energy. It is tempting to correlate this EQE roll-off to the Auger mechanism observed in optical measurements, but great caution needs to be applied before drawing such a conclusion. Indeed, the EQE roll-off was observed at very small current densities of 10 to 1000 mA cm^{-2} (Figure 2c), where the expected carrier concentration is likely significantly smaller than ≈10^{17} cm^{-3}, and hence unlikely large enough to cause Auger recombination. A strong limitation of quasi-2D PeLEDs is their severe EQE roll-off and low stability when driven electrically beyond a few tens of A cm^{-2}, even for high-<*n*> quasi-2D perovskites. To date, the most promising result is the demonstration of a stable PeLED operation up to 200 A cm^{-2} with an EQE of ≈0.3%.[92] Beyond 200 A cm^{-2}, irreversible degradation kicked in. The achieved *J* was still far below the threshold needed for electrically pumped ASE and lasing (≈4–10 kA cm^{-2}, as estimated by the authors), which might be due to the inferior charge transport and thermal

properties of quasi-2D perovskites, in addition to Auger recombination effects.

In contrast to quasi-2D perovskites, the lack of strong excitonic features in 3D perovskites leads to inferior EQEs in the low excitation regime. To enhance PLQY in the A cm^{-2} range, one can introduce bulky organic ligands such as benzylammonium iodide (PMAI) or ionic compounds such as potassium halides (KX) (Figure 2d).[78,93] Encouragingly, 3D PeLEDs were extensively investigated in the kA cm^{-2} range. To retain EQEs in this regime, it is necessary to tackle Joule heating, which is proportional to the dissipated electrical power and is exacerbated by poor thermal conductivities of non-epitaxial functional layers.

Several promising strategies can be employed to combat Joule heating. One approach involves engineering more conductive device stacks equipped with heat-sinking features.[89] For example, the voltage drop over typical organic transport layers can be reduced through interstitial doping of organic transport layers. However, only a small fraction of the dopant molecules contributes to free carrier conduction, while creating a large population of bound polaron states that have broad absorption bands.[94] Instead, these organic transport layers can be replaced with inorganic counterparts,[95,96] or nm-thick self-assembled monolayers.[97] Next, the amount of injected heat can be restricted by utilizing small active areas with electrical pulses featuring sharp edges.[89,90,98,99] Consequently, 3D PeLEDs approached 10 kA cm^{-2} when driven by electrical pulses with 1.2 ns rise times.[78] The highest current densities were enabled in a device geometry with reduced resistive-capacitance delay. Remarkably, neat $MAPbI_3$ perovskite outperformed other passivated emissive layers when comparing stabilized EL signals, showing that defect passivation plays a minor role at extreme J in the kA cm^{-2} range.

The build-up and dissipation of Joule heat in a PeLED based on a 150 nm-thick perovskite active layer can be quantified in a transient heat simulation (Figure 2e; Figure S1, Supporting Information). In our model, the exemplary PeLED is subjected to 1 µs-long current pulses spanning from 100 to 10 000 A cm^{-2}. The major heat accumulation takes place past ≈300 ns, wherein at $J > 1$ kA cm^{-2}, relevant for injection lasing,[90,92] the device heats by > 60 K. On the other hand, the increase is limited to just ≈10 K when using sub-10 ns electrical pulses. After the termination of the electrical pulse, it takes up to 100 µs to dissipate the thermal power, which favors the use of low-duty-cycle electrical pulses with a frequency of up to 10 kHz. By allowing PeLEDs to return to equilibrium, it was possible to preserve the EL across hundreds of thousands of intense (1 kA cm^{-2}) pulses.[78,100] We note that Joule heating is exacerbated for thicker perovskite emissive layers, hence favoring thinner structures to limit junction temperature.[101] Moreover, heat management is instrumental in decoupling Joule heating from other effects that influence EQE roll-off.[90]

Finally, cryogenic cooling of perovskite devices has resulted in significant benefits relevant to injection lasing. Lower temperatures have particularly been beneficial for the exponential reduction of ASE thresholds in 3D perovskites,[45,79] wherein a stronger threshold temperature dependence than $T^{3/2}$ was assigned to shallow band tails.[79] On the contrary, temperature dependence may be less pronounced in confined systems due to their sparse density of states.[102] Next, lower perovskite temperatures may enhance k_2,[76,77,103] yielding ever-increasing EQEs at lower temperatures. For example, a more than 4-fold brightness enhancement was achieved when reducing the device operating temperature to 77 K.[100] Additionally, lower temperatures allowed for the modulation of the dynamic charge balance inside the PeLED by controllable DC-bias-induced redistribution of mobile ions (Figure 2f), though this benefit gradually diminished toward extreme current densities. Overall, perovskite semiconductors have proven to operate very robustly at cryogenic temperatures, but it should be said that not all charge transport layers are suitable in such conditions. Materials with strongly temperature-dependent electrical conductivity, such as in particular many organic semiconductors, are less suitable. Furthermore, attention should be spent on the occurrence of phase transitions, which may impact k_3.[75]

4. From PeLEDs to Functional Electrical Waveguides

The high refractive indices (> 2) of perovskites compared to colloidal QDs and organic semiconductors facilitate lateral light amplification, orthogonal to the current injection in relatively thin vertical light-emitting devices. Surrounded by lower-index transport layers and electrodes, waveguide cores of perovskites can exhibit high mode confinement (Γ), which is defined as the ratio between optical power in the gain medium to the total optical power across the structure. In pursuit of low-threshold stimulated emission, these cladding layers should be characterized by low extinction coefficients.

In an electrically pumped device, the threshold current density (J_{th}) for stimulated emission can be estimated from the following equation, assuming balanced concentrations of electrons and holes and the dominant role of free-carrier radiative recombination:[90]

$$J_{th} = \frac{q\, d\, N_{th}}{\tau_{carrier}\, IQE} = \frac{q\, d\, k_2\, N_{th}^2}{IQE} \tag{5}$$

where q is the elementary charge. Even though thinner device structures would deliver lower J_{th}, the use of thin active media in optically lossy structures would necessitate higher carrier injection (higher g_i) to reach non-negative g_{net} (Note S1, Supporting Information). Neglecting scattering, self-absorption, and other losses, g_{net} can be linked to g_i via Γ and modal loss associated with the claddings (α_c):[104,105]

$$g_{net} = \Gamma g_i - \alpha_c \tag{6}$$

Optical propagation losses depend on guided mode overlap with the absorbing layers (calculated in Figure S2, Supporting Information) and remain relevant for far-from-unity Γ. In conventional PeLEDs optimized toward efficient EL operation (**Figure 3a**), the use of conductive transport layers and injection electrodes contributes to a high a_c. Consequently, a central challenge in creating a perovskite laser diode is to sustain LED operation while simultaneously mitigating optical losses.

Multiple strategies were proposed to tackle optical losses in electrically contacted LEDs, in which the active layer acts as a waveguide. In one approach, the recombination zone was moved away from the lossy electrodes by relying on lateral conduction in

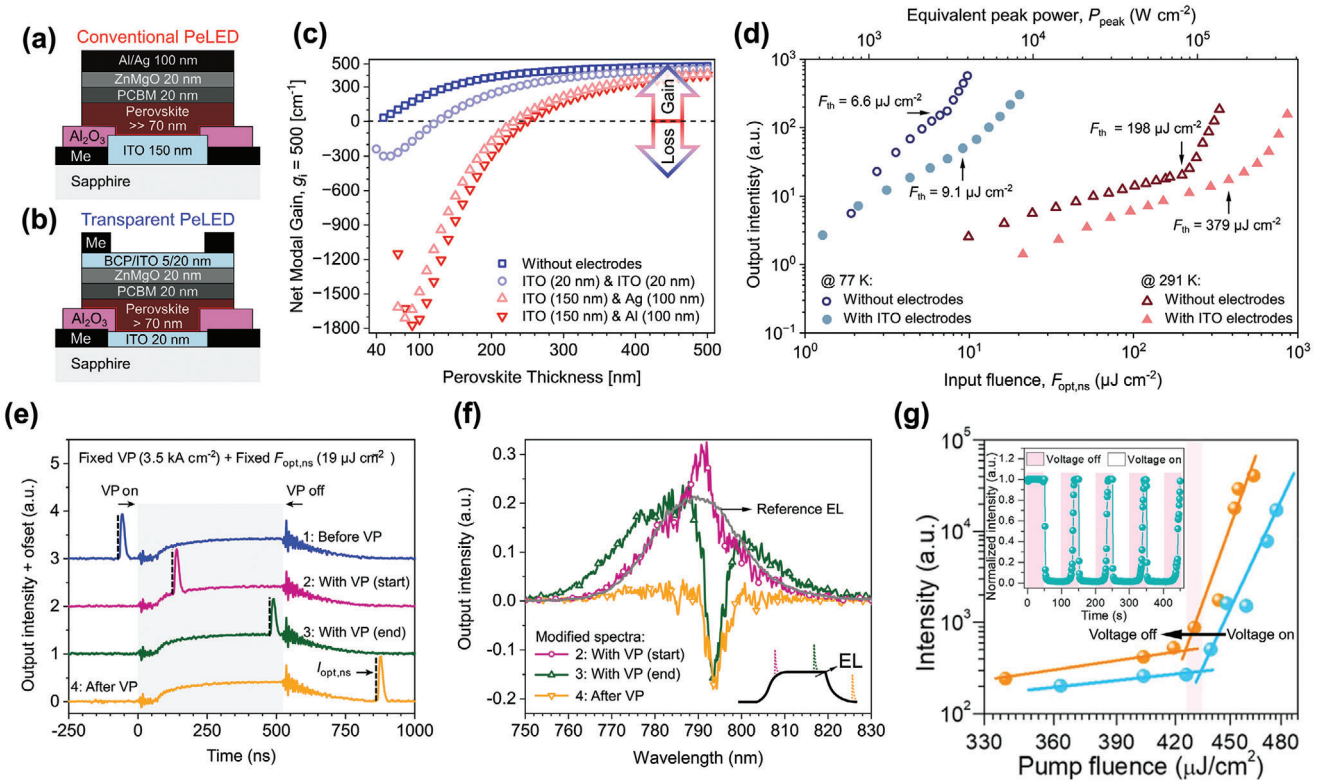

Figure 3. Modal properties of electrically contacted perovskite waveguiding devices. a) Schematics of a conventional PeLED structure with thick and optically lossy contact layers. b) Schematics of a transparent PeLED structure based on 20 nm-thick ITO contacts. Me: metal layer. No bottom transport layer was included in the model. Material constants and descriptions used for the simulation are listed in Table S3 (Supporting Information). Dimensions are not to scale. c) g_{net} simulation of four different waveguide structures as a function of perovskite thickness for exemplary g_i of 500 cm^{-1}. In the ultimate perovskite thickness limit, g_{net} will approach g_i in each architecture. The re-absorption in the perovskite was set to 0. d) ASE thresholds for a scaled PeLED (50 μm in diameter) and an electrode-free stack, measured at RT and 77 K. $F_{opt,ns}$: energy fluence under ns-excitation. e) Transient luminescence response produced using photo-electrical co-excitation of a scaled PeLED (50 μm in diameter) at 77 K. VP: voltage pulse. f) Corresponding spectral changes. Figures d–f) were reproduced with permission.[109] Copyright 2024, Springer Nature. g) Lasing input-output curves for a metal-insulator-perovskite structure with and without voltage bias. Inset: Temporal evolution of lasing intensity as a function of voltage bias applied on the second scale. Reproduced with permission.[110] Copyright 2021, American Chemical Society.

doped organic layers.[106] Similarly, a field-effect transistor configuration was explored to concentrate recombination to a narrow electrode-free zone.[107] Alternatively, the waveguide mode in a vertical LED structure can be separated by incorporating optically thick cladding layers.[108] However, limited mobilities of thin-film functional layers have restricted the attainable J and resulted in rather poor EQEs.

To replace absorbing electrodes, we highlight a promising strategy that exploits thin low-loss contact layers.[111] These contact layers, preferably of transparent conductive oxides such as indium tin oxide (ITO), can be placed in the immediate proximity of the gain layer with minimized thickness, while not greatly elevating free-carrier absorption losses (Figure 3b). By optimizing the indium-tin ratio and deposition conditions, one can tailor the ITO refractive index and transparency around the gain bandwidth.[112] The impact of perovskite film thickness and contact layers on the optical losses can be assessed by a numerical simulation of several device architectures. Assuming a reasonable g_i of 500 cm^{-1}, the optical losses induced by the transport layers are offset by utilizing a 50 nm-thick perovskite gain layer (Figure 3c). This is in stark contrast to conventional waveguide structures with a thick ITO anode and opaque cathodes. There, the thickness of a perovskite layer needs to exceed 200 nm to achieve a positive g_{net}. On the other hand, a transparent stack largely circumvents optical losses, where $g_{net} > 0$ is achieved for perovskite layers of 130 nm. This is despite largely similar Γ in all four waveguide geometries (Figure S2, Supporting Information). A transparent waveguide structure can support ASE at a comparatively lower J using a thinner active medium.

These mode simulations did not account for self-absorption of stimulated photons in unpumped gain medium regions, a phenomenon that can be pronounced in perovskites with a small Stokes shift. This loss channel is minuscule in optical excitation experiments where the entire perovskite excitation volume gets inverted following an exponential single-pass laser absorption profile, provided the layer is not excessively thick.[113] In contrast, in electrical devices charge carriers are typically less uniformly distributed across the gain medium, leaving a sizeable volume absorptive.[114] The difference in the recombination zone profile might contribute to a higher electrical pumping threshold relative to optical excitation and demands proper consideration.

The electrical performance of the proposed transparent architecture was validated in an LED stack with a 3D perovskite active layer (150 nm) sandwiched between thin (20 nm) transparent ITO electrodes in a current-focusing architecture using a 50 µm circular opening in a dielectric layer.[109] At 77 K, the PeLED delivered a high J (> 3 kA cm^{-2}) and was characterized by an F_{th} of 9.1 µJ cm^{-2} (N_{th} of ≈7.3 × 10^{17} cm^{-3}) when excited using ns-long optical pulses. In contrast, an electrode-free waveguide required an F_{th} of 6.6 µJ cm^{-2} (Figure 3d). By combining optical and electrical excitation of such a PeLED at 77 K, an F_{th} reduction of 13% was observed when the optical pulse was superimposed with the rising edge (first 50 ns) of the electrical pulse (Figure 3e,f). By the end of the 500 ns electrical pulse, the device temperature increased by more than 50 K (see Figure 2e), which led to a pronounced ASE signal quenching. A major drawback associated with such a transparent structure is an excessive resistive-capacitive delay that limited the rise time to ≈200 ns. The delay issue can be overcome by transitioning from dielectric pixel definition layers to more sophisticated electrode layouts.[78,99] More recently, combined optical and electrical excitation was applied to an LED equipped with a resonant cavity, where the electrical assist to lasing was limited to the first few ns of the electrical pulse, leading to a ≈24% threshold reduction relative to optical-only excitation.[115] These findings further show that photo-electrical co-excitation experiments can be used as a gauge to measure the progress toward a purely electrically pumped perovskite laser.

Several other studies unveiled the influence of electrical bias on optical ASE/lasing in different vertical and lateral PeLED and capacitor structures.[110,116] Although most reports observed a quenching of spontaneous and stimulated intensities upon applying an electric field, it has been shown that mobile ions can enhance ASE intensity in $CsPbBr_3$ perovskite.[117] This reversible effect was pronounced over timescales ranging from seconds to minutes (Figure 3g). Strategies to minimize N_{th} through the distribution of slow ions might accelerate the development of perovskite laser diodes.

5. Optical Cavity Integration into Light-Emitting Devices

The intensity of a guided mode can be strongly amplified through the integration of an optical resonator. Optically pumped lasing was measured experimentally in several perovskite systems featuring different resonant cavities such as nanowires,[118,119] nanoplates,[120] and microspheres.[121,122] The latter whispering gallery mode (WGM) resonators with their potentially extraordinary high quality factors (Q_{cav}) are very attractive as was also demonstrated for a standalone patterned $MAPbI_3$ microdisk.[123] The choice of cavity geometry affects the beam shape, emission wavelength and linewidth, mode operation, and, notably, the lasing threshold. To optimize laser cavities for low lasing threshold pump powers (P_{th}) or J_{th}, it is essential to consider the dependencies on cavity volume (V), cavity photon lifetime (τ_p), PLQY, and the quality factor of the emitter (Q_{em}). The latter is defined as the ratio of the central emission wavelength to the corresponding spontaneous emission linewidth. Q_{em} should not be confused with the Q_{cav} of the resonator, which is directly proportional to the photon lifetime. The dependence of threshold characteristics on these parameters follows the equation:[124]

$$J_{th} \propto P_{th} \propto \frac{1}{\mathrm{PLQY} \times Q_{em}} \times \frac{V}{\tau_p} \tag{7}$$

While the material parameters, specifically PLQY and Q_{em}, are very similar for a wide range of perovskites and thus not good selection criteria, τ_p and V are accessible by design and can be tuned across many orders of magnitude. Therefore, achieving injection lasing might turn out to be more accessible than cavity-free electrically stimulated ASE, as the photon lifetime within a resonator – and consequently within the gain medium – is extended. Additionally, it has been shown in optical pumping experiments that the ASE threshold decreases as the excitation length increases since the threshold corresponds to a certain required gain-length product.[125,126] For electrically pumped structures, the problem with long excitation lengths is that they demand a larger device size, which inevitably will suffer from higher temperatures by Joule heating when pumped to a certain N_{th} as compared to a shorter, smaller device. However, when a cavity is integrated with the waveguide, the required amplification length are strongly reduced compared to that of a planar structure.[113] This translates to a lower J_{th} for lasing, as well as a shorter physical gain length, hence a more compact device that will suffer less from Joule heating. It is an important prerequisite that none of the resonator design choices add optical or electrical losses to the system.

For a wide range of resonators, especially DFB cavities, the amount of power that is coupled back into the laser cavity, or the feedback strength, can be engineered through modification of grating features.[113,127] This design sensitivity of cavity parameters provides an extra degree of freedom to reduce the lasing threshold manyfold below the steady ASE threshold (**Figure 4a**). Similar benefits are expected from single-mode, e.g., high-Q_{cav} WGM cavities, especially when their resonant modes are tuned to the peak of the gain bandwidth. While WGM cavities can be fabricated with small radii and thus small resonator volumes, too high bending curvatures increase mode losses, thereby reducing the photon lifetime.[128]

Even though cavity architectures such as DFBs and disk resonators have shown potential for low-threshold lasing, the methods to ensure uniform and efficient current injection are yet to be developed to bring such structures from lasing under optical pumping to electrical pumping. Electrical devices with integrated cavities have been realized using DFB structures. DFB optical lasing was achieved in functional PeLED devices upon imprinting the perovskite gain layer or by etching cavity into the ITO anode (Figure 4b,c).[129] Alternatively, the insulating periodic DFB layer was used to induce complex index-gain coupling in scaled PeLED structures.[78] However, it is expected that a thin-film diode processed on a non-planar surface would suffer from increased leakage currents, strong local electric fields, device instability, and nonuniform current distribution. Nonetheless, such PeLEDs with integrated cavities allowed for J in excess of 10 kA cm^{-2} and delivered highly directional EL (Figure 4d).[78] A promising next step would be to maintain a high optical feedback strength of the cavity while preserving the electrical performance of planar LEDs.

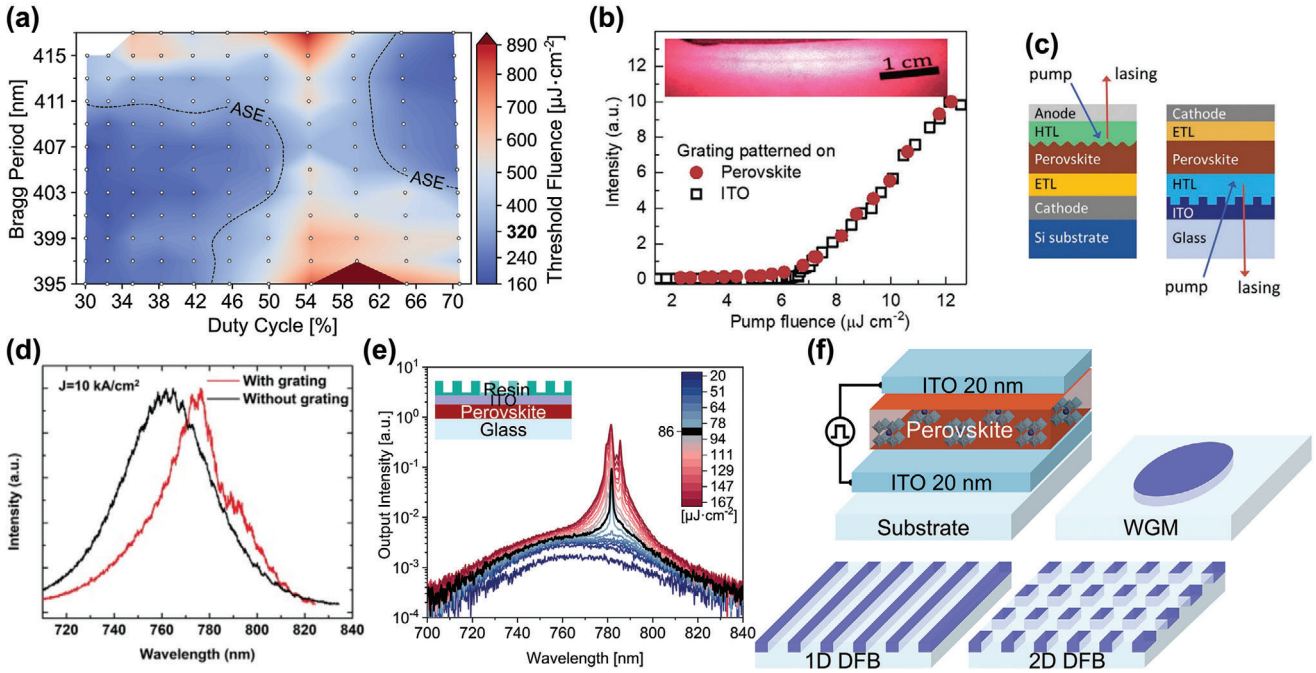

Figure 4. Perovskite waveguides and light-emitting devices with integrated resonators. All measurements were at RT. a) DFB lasing threshold extracted from a standalone perovskite film as a function of Bragg period and duty cycle under ns optical excitation. Dashed contours highlight the steady ASE threshold. Reproduced with permission.[113] Copyright 2024, John Wiley and Sons. b) Input-output lasing characteristics of top- and bottom-emitting LEDs shown in c) under ps optical excitation. Reproduced with permission.[129] Copyright 2019, John Wiley and Sons. d) EL spectra at J of 10 kA cm^{-2} of ns-pulsed PeLEDs with and without DFB cavity. Reproduced with permission.[78] Copyright 2021, John Wiley and Sons. e) Photoluminescence spectra of a UV-nanoimprinted DFB laser with a 20 nm-thick ITO interlayer under ns optical excitation. Inset: Waveguide structure. Reproduced with permission.[130] Copyright 2023, American Chemical Society. The waveguides in (a)-(e) incorporated second-order 1D DFB cavities. f) Proposed planar laser diode architecture with a cavity integrated into the lossless substrate. Dimensions are not to scale.

The integration of fully planar electrical stacks with variable resonator geometries combines the benefits of homogeneous electrical injection and a wider range of perovskite device fabrication techniques. One implementation is the monolithic integration of a feedback resonator above the perovskite active layer to enable pure index coupling.[130] To facilitate sufficient mode coupling, the optical distance between the gain medium and the grating needs to be minimized. Nonetheless, optically pumped lasing was achieved even when a 20 nm-thick ITO was inserted in between the active layer and grating (Figure 4e), making this approach promising when combined with a transparent architecture outlined in the previous section (Figure 3b). Alternatively, the resonators can be integrated into the substrate with a planarized arrangement of DFB or circular patterns of alternating materials with a refractive index difference (Figure 4f). By adopting this approach, high-precision semiconductor lithography processes can be utilized for the definition of resonator features prior to depositing fragile non-epitaxial functional layers. Furthermore, a completely planar device configuration would not affect current injection, which relaxes optical and electrical design constraints.

6. Conclusion

In this Perspective, we highlighted the critical developments that should enable the first demonstration of electrically pumped lasing from metal halide perovskites. In search of novel material compositions, researchers should focus on perovskite gain layers with low ASE thresholds that maintain their EL performance when driven electrically in an LED structure. Stable operation at high current densities (hundreds to thousands of A cm^{-2}) is likely required. We urge the community to characterize optical properties such as ASE or lasing threshold and optical gain using long optical excitations (ns to CW regime), and not limit them to the ps or fs regime. Indeed, electrical pumping sources will operate at ns and CW time scales, rather than in deep sub-ns regime.

At these time scales, several extra PLQY quenching mechanisms are activated and must be managed to reach electrically pumped lasing. Among them is Auger recombination, which can compete with stimulated emission. This carrier loss mechanism is particularly problematic in 0D perovskites, limiting their PLQY long before stimulated emission N_{th} can be established. Auger recombination is also a reported issue in quasi-2D perovskites, as it seems to already limit performance at moderate mean carrier densities, likely due to higher carrier concentrations in low-bandgap regions.

Encouragingly, quasi-2D and 3D perovskite semiconductors have repeatedly been brought to lasing under CW optical stimuli. At present, to unlock the potential of quasi-2D perovskites for injection lasing, it is essential to improve PeLED performance at higher current densities. However, due to the challenges of heat generation, Auger recombination, and device stability, their performance in the kA cm^{-2} range will likely remain limited. A more viable route relies on engineering quasi-2D perovskites with

reduced ASE thresholds through manipulating <*n*> and the organic cation of an active layer. 3D PeLEDs, in contrast, have overall inferior EQEs at low current densities but have an edge at high current densities. Several reports have shown operation at current densities of 1 to 10 kA cm^{-2} with decent EQEs. This was enabled in current-focusing architectures with elaborate thermal management. Moreover, such devices delivered enhanced EL performance at cryogenic temperatures that are also beneficial toward reduced ASE and lasing thresholds. Optical pumping experiments show that the ASE threshold increase can be limited to only ≈50% for a functional 3D PeLED with transparent electrodes compared to contact-free waveguides. Though electrically pumped ASE with PeLEDs has not been demonstrated yet, it is expected to be achievable with the currently known techniques and materials.

Integration of an optical cavity, which does not compromise PeLED performance, is a critical final step in developing a perovskite laser diode. In contrast to material parameters that are more challenging to manipulate, the design and features of a cavity can significantly affect the lasing threshold. Special attention should be paid to specific resonator structures that can be integrated with a thin-film diode, with DFB cavities and ring resonators emerging as the most feasible solutions. We note that well-designed feedback architectures can lower the threshold for lasing below the ASE threshold. The best marriage between an optical resonator structure and a PeLED may be achieved by embedding the optical cavity structure in the substrate, as it will simultaneously provide optical feedback and enable the seamless fabrication of a flat PeLED on top. This approach solves many challenges typically encountered during the fabrication of a thin light-emitting device atop a non-planarized optical grating. Moreover, by limiting advanced photolithography steps and associated harsh solvents to the substrate, performance of the thin-film stack would remain unaffected.

Supporting Information

Supporting Information is available from the Wiley Online Library or from the author.

Acknowledgements

I.G. and K.E. contributed equally to the work. The authors acknowledge funding from the European Research Council under the European Horizon 2020 Programme/ERC grant agreement no. 835133 (ULTRA-LUX). The authors thank Jiajun Qin from Linköping University (Sweden) for his insight and suggestions.

Conflict of Interest

I.G., K.E., N.A., R.G., J.G., and P.H. have a patent pending for the proposed planar LED structure with integrated resonators, with an application number EP23180095.4.

Keywords

amplified spontaneous emission, high current density, injection lasing, laser diode, metal halide perovskites, optical cavity

Received: December 26, 2023
Revised: June 17, 2024
Published online: August 23, 2024

[1] T. Komljenovic, M. Davenport, J. Hulme, A. Y. Liu, C. T. Santis, A. Spott, S. Srinivasan, E. J. Stanton, C. Zhang, J. E. Bowers, *J. Lightwave Technol.* **2016**, *34*, 20.
[2] W. B. Gunnarsson, K. Roh, L. Zhao, J. P. Murphy, A. J. Grede, N. C. Giebink, B. P. Rand, *Chem. Rev.* **2023**, *123*, 7548.
[3] L. N. Quan, B. P. Rand, R. H. Friend, S. G. Mhaisalkar, T. W. Lee, E. H. Sargent, *Chem. Rev.* **2019**, *119*, 7444.
[4] B. R. Sutherland, E. H. Sargent, *Nat. Photonics* **2016**, *10*, 295.
[5] J. Roh, Y. S. Park, J. Lim, V. I. Klimov, *Nat. Commun.* **2020**, *11*, 271.
[6] A. S. D. Sandanayaka, T. Matsushima, F. Bencheikh, K. Yoshida, M. Inoue, T. Fujihara, K. Goushi, J.-C. Ribierre, C. Adachi, *Sci. Adv.* **2017**, *3*, 1602570.
[7] X. Tang, C. A. M. Senevirathne, T. Matsushima, A. S. D. Sandanayaka, C. Adachi, *Adv. Mater.* **2023**, *36*, 2211873.
[8] F. Zhao, A. Ren, P. Li, Y. Li, J. Wu, Z. M. Wang, *ACS Nano* **2021**, *16*, 6943.
[9] Q. Zhang, W. Tao, J. Huang, R. Xia, J. Cabanillas-Gonzalez, *Adv. Photonics Res.* **2021**, *2*, 2000155.
[10] N. Ahn, Y. S. Park, C. Livache, J. Du, K. Gungor, J. Kim, V. I. Klimov, *Adv. Mater.* **2023**, *35*, 2206613.
[11] N. Ahn, C. Livache, V. Pinchetti, H. Jung, H. Jin, D. Hahm, Y.-S. Park, V. I. Klimov, *Nature* **2023**, *617*, 79.
[12] A. S. D. Sandanayaka, T. Matsushima, F. Bencheikh, S. Terakawa, W. J. Potscavage, C. Qin, T. Fujihara, K. Goushi, J. C. Ribierre, C. Adachi, *Appl. Phys. Express* **2019**, *12*, 061010.
[13] K. Yoshida, J. Gong, A. L. Kanibolotsky, P. J. Skabara, G. A. Turnbull, I. D. W. Samuel, *Nature* **2023**, *621*, 746.
[14] T. Zhang, F. Wang, H.-B. Kim, I.-W. Choi, C. Wang, E. Cho, R. Konefal, Y. Puttisong, K. Terado, L. Kobera, M. Chen, M. Yang, S. Bai, B. Yang, J. Suo, S.-C. Yang, X. Liu, F. Fu, H. Yoshida, W. M. Chen, J. Brus, V. Coropceanu, A. Hagfeldt, J.-L. Brédas, M. Fahlman, D. Suk Kim, Z. Hu, F. Gao, *Science* **2022**, *377*, 495.
[15] H. Lu, Y. Liu, P. Ahlawat, A. Mishra, W. R. Tress, F. T. Eickemeyer, Y. Yang, F. Fu, Z. Wang, C. E. Avalos, B. I. Carlsen, A. Agarwalla, X. Zhang, X. Li, Y. Zhan, S. M. Zakeeruddin, L. Emsley, U. Rothlisberger, L. Zheng, A. Hagfeldt, M. Grätzel, *Science* **2020**, *370*, abb8985.
[16] R. Lin, J. Xu, M. Wei, Y. Wang, Z. Qin, Z. Liu, J. Wu, K. Xiao, B. Chen, S. M. Park, G. Chen, H. R. Atapattu, K. R. Graham, J. Xu, J. Zhu, L. Li, C. Zhang, E. H. Sargent, H. Tan, *Nature* **2022**, *603*, 73.
[17] B. Guo, R. Lai, S. Jiang, L. Zhou, Z. Ren, Y. Lian, P. Li, X. Cao, S. Xing, Y. Wang, W. Li, C. Zou, M. Chen, Z. Hong, C. Li, B. Zhao, D. Di, *Nat. Photonics* **2022**, *16*, 637.
[18] J. S. Kim, J. M. Heo, G. S. Park, S. J. Woo, C. Cho, H. J. Yun, D. H. Kim, J. Park, S. C. Lee, S. H. Park, E. Yoon, N. C. Greenham, T. W. Lee, *Nature* **2022**, *611*, 688.
[19] H. Wang, F. U. Kosasih, H. Yu, G. Zheng, J. Zhang, G. Pozina, Y. Liu, C. Bao, Z. Hu, X. Liu, L. Kobera, S. Abbrent, J. Brus, Y. Jin, M. Fahlman, R. H. Friend, C. Ducati, X. K. Liu, F. Gao, *Nat. Commun.* **2020**, *11*, 891.
[20] A. Fakharuddin, M. K. Gangishetty, M. Abdi-Jalebi, S. H. Chin, A. R. bin Mohd Yusoff, D. N. Congreve, W. Tress, F. Deschler, M. Vasilopoulou, H. J. Bolink, *Nat. Electron.* **2022**, *5*, 203.
[21] R. Ollearo, J. Wang, M. J. Dyson, C. H. L. Weijtens, M. Fattori, B. T. van Gorkom, A. J. J. M. van Breemen, S. C. J. Meskers, R. A. J. Janssen, G. H. Gelinck, *Nat. Commun.* **2021**, *12*, 7277.

[22] F. Wang, X. Zou, M. Xu, H. Wang, H. Wang, H. Guo, J. Guo, P. Wang, M. Peng, Z. Wang, Y. Wang, J. Miao, F. Chen, J. Wang, X. Chen, A. Pan, C. Shan, L. Liao, W. Hu, *Adv. Sci.* **2021**, *8*, 2100569.
[23] L. M. Herz, *ACS Energy Lett.* **2017**, *2*, 1539.
[24] J. M. Richter, M. Abdi-Jalebi, A. Sadhanala, M. Tabachnyk, J. P. H. Rivett, L. M. Pazos-Outón, K. C. Gödel, M. Price, F. Deschler, R. H. Friend, *Nat. Commun.* **2016**, *7*, 13941.
[25] C. La-O-Vorakiat, T. Salim, J. Kadro, M. T. Khuc, R. Haselsberger, L. Cheng, H. Xia, G. G. Gurzadyan, H. Su, Y. M. Lam, R. A. Marcus, M. E. Michel-Beyerle, E. E. M. Chia, *Nat. Commun.* **2015**, *6*, 7903.
[26] D. A. Tatarinov, S. S. Anoshkin, I. A. Tsibizov, V. Sheremet, F. Isik, A. Y. Zhizhchenko, A. B. Cherepakhin, A. A. Kuchmizhak, A. P. Pushkarev, H. V. Demir, S. V. Makarov, *Adv. Opt. Mater.* **2023**, *11*, 2202407.
[27] K. Elkhouly, I. Goldberg, H. G. Boyen, A. Franquet, V. Spampinato, T. H. Ke, R. Gehlhaar, J. Genoe, J. Hofkens, P. Heremans, W. Qiu, *Adv. Opt. Mater.* **2021**, *9*, 2100586.
[28] Q. Dong, L. Lei, J. Mendes, F. So, *J. Phys.: Mater.* **2020**, *3*, 012002.
[29] T. Cheng, G. Tumen-Ulzii, D. Klotz, S. Watanabe, T. Matsushima, C. Adachi, *ACS Appl. Mater. Interfaces* **2020**, *12*, 33004.
[30] L. Zhao, R. A. Kerner, Z. Xiao, Y. L. Lin, K. M. Lee, J. Schwartz, B. P. Rand, *ACS Energy Lett.* **2016**, *1*, 595.
[31] J. Hu, Z. Xu, T. L. Murrey, I. Pelczer, A. Kahn, J. Schwartz, B. P. Rand, *Adv. Mater.* **2023**, *35*, 2303373.
[32] L. Lei, Q. Dong, K. Gundogdu, F. So, *Adv. Funct. Mater.* **2021**, *31*, 2010144.
[33] S. Feldmann, S. Macpherson, S. P. Senanayak, M. Abdi-Jalebi, J. P. H. Rivett, G. Nan, G. D. Tainter, T. A. S. Doherty, K. Frohna, E. Ringe, R. H. Friend, H. Sirringhaus, M. Saliba, D. Beljonne, S. D. Stranks, F. Deschler, *Nat. Photonics* **2020**, *14*, 123.
[34] L. Zhang, C. Sun, T. He, Y. Jiang, J. Wei, Y. Huang, M. Yuan, *Light: Sci. Appl.* **2021**, *10*, 61.
[35] Y. Jiang, J. Wei, M. Yuan, *J. Phys. Chem. Lett.* **2021**, *12*, 2593.
[36] L. Protesescu, S. Yakunin, M. I. Bodnarchuk, F. Krieg, R. Caputo, C. H. Hendon, R. X. Yang, A. Walsh, M. V. Kovalenko, *Nano Lett.* **2015**, *15*, 3692.
[37] H. C. Wang, Z. Bao, H. Y. Tsai, A. C. Tang, R. S. Liu, *Small* **2018**, *14*, 1702433.
[38] Y. F. Li, J. Feng, H. B. Sun, *Nanoscale* **2019**, *11*, 19119.
[39] P. Geiregat, J. Maes, K. Chen, E. Drijvers, J. De Roo, J. M. Hodgkiss, Z. Hens, *ACS Nano* **2018**, *12*, 10178.
[40] J. Butkus, P. Vashishtha, K. Chen, J. K. Gallaher, S. K. K. Prasad, D. Z. Metin, G. Laufersky, N. Gaston, J. E. Halpert, J. M. Hodgkiss, *Chem. Mater.* **2017**, *29*, 3644.
[41] Y. Jia, R. A. Kerner, A. J. Grede, B. P. Rand, N. C. Giebink, *Nat. Photonics* **2017**, *11*, 784.
[42] C. Qin, A. S. D. Sandanayaka, C. Zhao, T. Matsushima, D. Zhang, T. Fujihara, C. Adachi, *Nature* **2020**, *585*, 53.
[43] N. Ahn, C. Livache, V. Pinchetti, V. I. Klimov, *Chem. Rev.* **2023**, *123*, 8251.
[44] G. Xing, N. Mathews, S. S. Lim, N. Yantara, X. Liu, D. Sabba, M. Grätzel, S. Mhaisalkar, T. C. Sum, *Nat. Mater.* **2014**, *13*, 476.
[45] P. Brenner, O. Bar-On, M. Jakoby, I. Allegro, B. S. Richards, U. W. Paetzold, I. A. Howard, J. Scheuer, U. Lemmer, *Nat. Commun.* **2019**, *10*, 988.
[46] I. Tanghe, M. Samoli, I. Wagner, S. A. Cayan, A. H. Khan, K. Chen, J. Hodgkiss, I. Moreels, D. Van Thourhout, Z. Hens, P. Geiregat, *Nat. Nanotechnol.* **2023**, *18*, 1423.
[47] Y. Yamada, T. Nakamura, M. Endo, A. Wakamiya, Y. Kanemitsu, *J. Am. Chem. Soc.* **2014**, *136*, 11610.
[48] V. D'Innocenzo, G. Grancini, M. J. P. Alcocer, A. R. S. Kandada, S. D. Stranks, M. M. Lee, G. Lanzani, H. J. Snaith, A. Petrozza, *Nat. Commun.* **2014**, *5*, 3586.
[49] S. Nah, B. Spokoyny, C. Stoumpos, C. M. M. Soe, M. Kanatzidis, E. Harel, *Nat. Photonics* **2017**, *11*, 285.
[50] R. Tomar, A. Kulkarni, K. Chen, S. Singh, D. Van Thourhout, J. M. Hodgkiss, L. D. A. Siebbeles, Z. Hens, P. Geiregat, *J. Phys. Chem. C* **2019**, *123*, 9640.
[51] V. I. Klimov, S. A. Ivanov, J. Nanda, M. Achermann, I. Bezel, J. A. McGuire, A. Piryatinski, *Nature* **2007**, *447*, 441.
[52] N. Taghipour, M. Dalmases, G. L. Whitworth, M. Dosil, A. Othonos, S. Christodoulou, S. M. Liga, G. Konstantatos, *Adv. Mater.* **2023**, *35*, 202207678.
[53] K. Wu, Y. S. Park, J. Lim, V. I. Klimov, *Nat. Nanotechnol.* **2017**, *12*, 1140.
[54] Z. Liu, Y. Bekenstein, X. Ye, S. C. Nguyen, J. Swabeck, D. Zhang, S. T. Lee, P. Yang, W. Ma, A. P. Alivisatos, *J. Am. Chem. Soc.* **2017**, *139*, 5309.
[55] J. S. Manser, J. A. Christians, P. V. Kamat, *Chem. Rev.* **2016**, *116*, 12956.
[56] S. Yakunin, L. Protesescu, F. Krieg, M. I. Bodnarchuk, G. Nedelcu, M. Humer, G. De Luca, M. Fiebig, W. Heiss, M. V. Kovalenko, *Nat. Commun.* **2015**, *6*, 8056.
[57] K. Fujiwara, S. Zhang, S. Takahashi, L. Ni, A. Rao, K. Yamashita, *ACS Photonics* **2020**, *7*, 845.
[58] J. C. Blancon, A. V. Stier, H. Tsai, W. Nie, C. C. Stoumpos, B. Traoré, L. Pedesseau, M. Kepenekian, F. Katsutani, G. T. Noe, J. Kono, S. Tretiak, S. A. Crooker, C. Katan, M. G. Kanatzidis, J. J. Crochet, J. Even, A. D. Mohite, *Nat. Commun.* **2018**, *9*, 2254.
[59] Y. Li, I. Allegro, M. Kaiser, A. J. Malla, B. S. Richards, U. Lemmer, U. W. Paetzold, I. A. Howard, *Mater. Today* **2021**, *49*, 35.
[60] L. Lei, D. Seyitliyev, S. Stuard, J. Mendes, Q. Dong, X. Fu, Y. A. Chen, S. He, X. Yi, L. Zhu, C. H. Chang, H. Ade, K. Gundogdu, F. So, *Adv. Mater.* **2020**, *32*, 1906571.
[61] A. L. Alvarado-Leaños, D. Cortecchia, G. Folpini, A. R. Srimath Kandada, A. Petrozza, *Adv. Opt. Mater.* **2021**, *9*, 2001773.
[62] N. Annavarapu, I. Goldberg, A. Papadopoulou, K. Elkhouly, J. Genoe, R. Gehlhaar, P. Heremans, *ACS Photonics* **2023**, *10*, 1583.
[63] C. Zhao, C. Qin, *Nanophotonics* **2021**, *10*, 2167.
[64] J. Moon, Y. Mehta, K. Gundogdu, F. So, Q. Gu, *Adv. Mater.* **2023**, *36*, 202211284.
[65] C. Cho, A. Palatnik, M. Sudzius, R. Grodofzig, F. Nehm, K. Leo, *ACS Appl. Mater. Interfaces* **2020**, *12*, 35242.
[66] J. Qin, Y. Tang, J. Zhang, T. Shen, M. Karlsson, T. Zhang, W. Cai, L. Shi, W. X. Ni, F. Gao, *Mater. Horiz.* **2023**, *10*, 1446.
[67] S. Milanese, M. L. De Giorgi, L. Cerdán, M. G. La-Placa, P. P. Boix, H. J. Bolink, M. Anni, *Mater. Today Proc.* **2022**, *67*, 959.
[68] J. Qin, X. K. Liu, C. Yin, F. Gao, *Trends Chem.* **2021**, *3*, 34.
[69] G. Delport, G. Chehade, F. Lédeé, H. Diab, C. Milesi-Brault, G. Trippé-Allard, J. Even, J. S. Lauret, E. Deleporte, D. Garrot, *J. Phys. Chem. Lett.* **2019**, *10*, 5153.
[70] H. Zhu, Y. Fu, F. Meng, X. Wu, Z. Gong, Q. Ding, M. V. Gustafsson, M. T. Trinh, S. Jin, X. Y. Zhu, *Nat. Mater.* **2015**, *14*, 636.
[71] N. S. Makarov, S. Guo, O. Isaienko, W. Liu, I. Robel, V. I. Klimov, *Nano Lett.* **2016**, *16*, 2349.
[72] J. A. Castañeda, G. Nagamine, E. Yassitepe, L. G. Bonato, O. Voznyy, S. Hoogland, A. F. Nogueira, E. H. Sargent, C. H. B. Cruz, L. A. Padilha, *ACS Nano* **2016**, *10*, 8603.
[73] T. C. Sum, M. Righetto, S. S. Lim, *J. Chem. Phys.* **2020**, *152*, 130901.
[74] C. Wehrenfennig, G. E. Eperon, M. B. Johnston, H. J. Snaith, L. M. Herz, *Adv. Mater.* **2014**, *26*, 1584.
[75] R. L. Milot, G. E. Eperon, H. J. Snaith, M. B. Johnston, L. M. Herz, *Adv. Funct. Mater.* **2015**, *25*, 6218.
[76] C. L. Davies, M. R. Filip, J. B. Patel, T. W. Crothers, C. Verdi, A. D. Wright, R. L. Milot, F. Giustino, M. B. Johnston, L. M. Herz, *Nat. Commun.* **2018**, *9*, 293.

[77] I. Allegro, Y. Li, B. S. Richards, U. W. Paetzold, U. Lemmer, I. A. Howard, *J. Phys. Chem. Lett.* **2021**, *12*, 2293.
[78] L. Zhao, K. Roh, S. Kacmoli, K. Al Kurdi, X. Liu, S. Barlow, S. R. Marder, C. Gmachl, B. P. Rand, *Adv. Mater.* **2021**, *33*, 2104867.
[79] Y. Jia, R. A. Kerner, A. J. Grede, B. P. Rand, N. C. Giebink, *Adv. Opt. Mater.* **2020**, *8*, 1901514.
[80] C. Qin, T. Matsushima, W. J. Potscavage, A. S. D. Sandanayaka, M. R. Leyden, F. Bencheikh, K. Goushi, F. Mathevet, B. Heinrich, G. Yumoto, Y. Kanemitsu, C. Adachi, *Nat. Photonics* **2020**, *14*, 70.
[81] M. Anaya, B. P. Rand, R. J. Holmes, D. Credgington, H. J. Bolink, R. H. Friend, J. Wang, N. C. Greenham, S. D. Stranks, *Nat. Photonics* **2019**, *13*, 818.
[82] S. D. Stranks, R. L. Z. Hoye, D. Di, R. H. Friend, F. Deschler, *Adv. Mater.* **2018**, *31*, 1803336.
[83] K. Lin, J. Xing, L. N. Quan, F. P. G. de Arquer, X. Gong, J. Lu, L. Xie, W. Zhao, D. Zhang, C. Yan, W. Li, X. Liu, Y. Lu, J. Kirman, E. H. Sargent, Q. Xiong, Z. Wei, *Nature* **2018**, *562*, 245.
[84] Y. Hassan, J. H. Park, M. L. Crawford, A. Sadhanala, J. Lee, J. C. Sadighian, E. Mosconi, R. Shivanna, E. Radicchi, M. Jeong, C. Yang, H. Choi, S. H. Park, M. H. Song, F. De Angelis, C. Y. Wong, R. H. Friend, B. R. Lee, H. J. Snaith, *Nature* **2021**, *591*, 72.
[85] W. Xu, Q. Hu, S. Bai, C. Bao, Y. Miao, Z. Yuan, T. Borzda, A. J. Barker, E. Tyukalova, Z. Hu, M. Kawecki, H. Wang, Z. Yan, X. Liu, X. Shi, K. Uvdal, M. Fahlman, W. Zhang, M. Duchamp, J. M. Liu, A. Petrozza, J. Wang, L. M. Liu, W. Huang, F. Gao, *Nat. Photonics* **2019**, *13*, 418.
[86] B. Zhao, S. Bai, V. Kim, R. Lamboll, R. Shivanna, F. Auras, J. M. Richter, L. Yang, L. Dai, M. Alsari, X. J. She, L. Liang, J. Zhang, S. Lilliu, P. Gao, H. J. Snaith, J. Wang, N. C. Greenham, R. H. Friend, D. Di, *Nat. Photonics* **2018**, *12*, 783.
[87] Z. Yuan, Y. Miao, Z. Hu, W. Xu, C. Kuang, K. Pan, P. Liu, J. Lai, B. Sun, J. Wang, S. Bai, F. Gao, *Nat. Commun.* **2019**, *10*, 2818.
[88] Z. Liu, W. Qiu, X. Peng, G. Sun, X. Liu, D. Liu, Z. Li, F. He, C. Shen, Q. Gu, F. Ma, H. L. Yip, L. Hou, Z. Qi, S. J. Su, *Adv. Mater.* **2021**, *33*, 2103268.
[89] L. Zhao, K. Roh, S. Kacmoli, K. Al Kurdi, S. Jhulki, S. Barlow, S. R. Marder, C. Gmachl, B. P. Rand, *Adv. Mater.* **2020**, *32*, 2000752.
[90] H. Kim, L. Zhao, J. S. Price, A. J. Grede, K. Roh, A. N. Brigeman, M. Lopez, B. P. Rand, N. C. Giebink, *Nat. Commun.* **2018**, *9*, 4893.
[91] Y. Jiang, M. Cui, S. Li, C. Sun, Y. Huang, J. Wei, L. Zhang, M. Lv, C. Qin, Y. Liu, M. Yuan, *Nat. Commun.* **2021**, *12*, 336.
[92] M. R. Leyden, S. Terakawa, T. Matsushima, S. Ruan, K. Goushi, M. Auffray, A. S. D. Sandanayaka, C. Qin, F. Bencheikh, C. Adachi, *ACS Photonics* **2019**, *6*, 460.
[93] C. Zou, Y. Liu, D. S. Ginger, L. Y. Lin, *ACS Nano* **2020**, *14*, 6076.
[94] M. L. Tietze, J. Benduhn, P. Pahner, B. Nell, M. Schwarze, H. Kleemann, M. Krammer, K. Zojer, K. Vandewal, K. Leo, *Nat. Commun.* **2018**, *9*, 1182.
[95] Y. Jiang, L. Jiang, F. S. Yan Yeung, P. Xu, S. Chen, H. S. Kwok, G. Li, *ACS Appl. Mater. Interfaces* **2019**, *11*, 11119.
[96] J. M. Caruge, J. E. Halpert, V. Wood, V. Buloví, M. G. Bawendi, *Nat. Photonics* **2008**, *2*, 247.
[97] Z. Li, Z. Chen, Z. Shi, G. Zou, L. Chu, X. K. Chen, C. Zhang, S. K. So, H. L. Yip, *Nat. Commun.* **2023**, *14*, 6441.
[98] I. Goldberg, W. Qiu, K. Elkhouly, N. Annavarapu, A. N. Mehta, C. Rolin, T.-H. Ke, R. Gehlhaar, J. Genoe, P. Heremans, *J. Mater. Chem. C* **2021**, *9*, 12661.
[99] L. Zhao, D. D. Astridge, W. B. Gunnarsson, Z. Xu, J. Hong, J. Scott, S. Kacmoli, K. Al Kurdi, S. Barlow, S. R. Marder, C. F. Gmachl, A. Sellinger, B. P. Rand, *Nano Lett.* **2023**, *23*, 4785.
[100] K. Elkhouly, I. Goldberg, N. Annavarapu, R. Gehlhaar, T. H. Ke, J. Genoe, J. Hofkens, P. Heremans, W. Qiu, *Adv. Opt. Mater.* **2022**, *10*, 2200024.
[101] L. Zhao, K. M. Lee, K. Roh, S. U. Z. Khan, B. P. Rand, *Adv. Mater.* **2019**, *31*, 1805836.
[102] Z. Liu, J. Yang, J. Du, Z. Hu, T. Shi, Z. Zhang, Y. Liu, X. Tang, Y. Leng, R. Li, *ACS Nano* **2018**, *12*, 5923.
[103] Y. He, J. Yan, L. Xu, B. Zhang, Q. Cheng, Y. Cao, J. Zhang, C. Tao, Y. Wei, K. Wen, Z. Kuang, G. M. Chow, Z. Shen, Q. Peng, W. Huang, J. Wang, *Adv. Mater.* **2021**, *33*, 2006302.
[104] H. Ghafouri-Shiraz, *Principles of Semiconductor Laser Diodes and Amplifiers: Analysis and Transmission Line Laser Modeling*, World Scientific, **2003**.
[105] L. A. Coldren, S. W. Corzine, M. L. Mashanovitch, *Diode Lasers and Photonic Integrated Circuits*, 2nd ed., Wiley, New York **2012**.
[106] S. Schols, S. Verlaak, C. Rolin, D. Cheyns, J. Genoe, P. Heremans, *Adv. Funct. Mater.* **2008**, *18*, 136.
[107] J. H. Lee, T. H. Ke, J. Genoe, P. Heremans, C. Rolin, *Adv. Electron. Mater.* **2019**, *5*, 1800437.
[108] C. Cho, T. Antrack, M. Kroll, Q. An, T. R. Bärschneider, A. Fischer, S. Meister, Y. Vaynzof, K. Leo, *Adv. Sci.* **2021**, *8*, 2101663.
[109] K. Elkhouly, I. Goldberg, X. Zhang, N. Annavarapu, S. Hamdad, G. Croes, C. Rolin, J. Genoe, W. Qiu, R. Gehlhaar, P. Heremans, *Nat. Photonics* **2024**, *18*, 132.
[110] Y. Gao, X. Li, W. Liu, X. Xing, H. Long, K. Wang, B. Wang, P. Lu, *Nano Lett.* **2021**, *21*, 10230.
[111] H. Yamamoto, T. Oyamada, H. Sasabe, C. Adachi, *Appl. Phys. Lett.* **2004**, *84*, 1401.
[112] M. Balestrieri, D. Pysch, J. P. Becker, M. Hermle, W. Warta, S. W. Glunz, *Sol. Energy Mater. Sol. Cells* **2011**, *95*, 2390.
[113] N. Annavarapu, I. Goldberg, S. Hamdad, K. Elkhouly, R. Puybaret, D. Sabuncuoglu Tezcan, J. Genoe, R. Gehlhaar, P. Heremans, *Adv. Opt. Mater.* **2024**, 2302496.
[114] B. P. Rand, N. C. Giebink, *Nat. Photonics* **2024**, *18*, 107.
[115] A. J. Grede, R. Cawthorn, L. Zhao, J. P. Murphy, K. Roh, K. Al Kurdi, S. Barlow, S. R. Marder, B. P. Rand, N. C. Giebink, *ACS Photonics* **2024**, *11*, 1851.
[116] P. Liu, C. Gu, Q. Liao, *ACS Omega* **2021**, *6*, 34021.
[117] Y. Li, H. Hu, A. Farag, T. Feeney, I. Allegro, U. Lemmer, U. W. Paetzold, I. A. Howard, *Nano Lett.* **2023**, *23*, 1637.
[118] P. Liu, X. He, J. Ren, Q. Liao, J. Yao, H. Fu, *ACS Nano* **2017**, *11*, 5766.
[119] H. Zhu, Y. Fu, F. Meng, X. Wu, Z. Gong, Q. Ding, M. V. Gustafsson, M. T. Trinh, S. Jin, X. Y. Zhu, *Nat. Mater.* **2015**, *14*, 636.
[120] T. Wang, W. Yang, B. Li, R. Bian, X. Jia, H. Yu, L. Wang, X. Li, F. Xie, H. Zhu, J. Yang, Y. Gao, Q. Zhou, C. He, X. Liu, Y. Ye, *ACS Appl. Nano Mater.* **2020**, *3*, 12017.
[121] B. Zhou, Y. Zhong, M. Jiang, J. Zhang, H. Dong, L. Chen, H. Wu, W. Xie, L. Zhang, *Nanoscale* **2020**, *12*, 5805.
[122] B. Tang, H. Dong, L. Sun, W. Zheng, Q. Wang, F. Sun, X. Jiang, A. Pan, L. Zhang, *ACS Nano* **2017**, *11*, 10681.
[123] P. J. Cegielski, A. L. Giesecke, S. Neutzner, C. Porschatis, M. Gandini, D. Schall, C. A. R. Perini, J. Bolten, S. Suckow, S. Kataria, B. Chmielak, T. Wahlbrink, A. Petrozza, M. C. Lemme, *Nano Lett.* **2018**, *18*, 6915.
[124] J. B. Khurgin, M. A. Noginov, *Laser Photonics Rev.* **2021**, *15*, 2000250.
[125] G. I. Peters, L. Allen, *J. Phys., A* **1971**, *4*, 238.
[126] K. N. Bourdakos, L. A. Cury, A. P. Monkman, *Org. Electron.* **2011**, *12*, 1142.
[127] Q. Dong, X. Fu, D. Seyitliyev, K. Darabi, J. Mendes, L. Lei, Y. A. Chen, C. H. Chang, A. Amassian, K. Gundogdu, F. So, *ACS Photonics* **2022**, *9*, 3124.
[128] D. Parrain, C. Baker, G. Wang, B. Guha, E. G. Santos, A. Lemaitre, P. Senellart, G. Leo, S. Ducci, I. Favero, *Opt. Express* **2015**, *23*, 19656.
[129] H. Kim, K. Roh, J. P. Murphy, L. Zhao, W. B. Gunnarsson, E. Longhi, S. Barlow, S. R. Marder, B. P. Rand, N. C. Giebink, *Adv. Opt. Mater.* **2019**, *8*, 1901297.
[130] I. Goldberg, N. Annavarapu, S. Leitner, K. Elkhouly, F. Han, N. Verellen, T. Kuna, W. Qiu, C. Rolin, J. Genoe, R. Gehlhaar, P. Heremans, *ACS Photonics* **2023**, *10*, 1591.